Acta Crystallographica Section D
Biological Crystallography
ISSN 0907-4449

Crystallization and preliminary analysis of xenobiotic reductase A and ligand complexes from *Pseudomonas putida* II-B

Allen M. Orville,[a]* Linda Manning,[a] David S. Blehert,[b] Joey M. Studts,[c] Brian G. Fox[c] and Glenn H. Chambliss[b]

[a]School of Chemistry and Biochemistry, Georgia Institute of Technology, Atlanta, GA 30332-0400, USA, [b]Department of Bacteriology, University of Wisconsin, Madison, WI 53706, USA, and [c]Department of Biochemistry, College of Agricultural and Life Sciences, University of Wisconsin, Madison WI 53706-1544, USA

Correspondence e-mail: allen.orville@chemistry.gatech.edu

Received 31 December 2003
Accepted 15 March 2004

Diffraction-quality crystals have been obtained of the xenobiotic reductase A (XenA) from *Pseudomonas* II-B, which was originally cultured from the contaminated soil of a World War II era munitions-manufacturing plant. Several complete X-ray diffraction data sets have been collected and analyzed. The native XenA data set includes reflections between 35 and 1.65 Å. Four-wavelength MAD data sets from selenomethionine-enriched XenA and from three different ligand complexes are also reported. The XenA crystals belong to space group $P2_12_12$, with unit-cell parameters $a = 84$, $b = 158$, $c = 57$ Å. Experimental phasing from analysis of the MAD data from selenomethionine-enriched XenA reveals the presence of two molecules in the asymmetric unit. They are related by a non-crystallographic 2_1 screw axis nearly parallel to the c axis, but offset by a quarter unit-cell translation. Thus, the local symmetry produces approximate systematic absences along the (00l) principal axis and complicates the space-group determination.

1. Introduction

Microbes have evolved over billions of years to the point where they are now responsible for most of the transformations and flux of the chemical cycles in the biosphere (Mojzsis *et al.*, 1996; Falkowski *et al.*, 2000; Watanabe *et al.*, 2000; Nisbet & Sleep, 2001). The success and ubiquity of bacteria arises from their ability to metabolize diverse compounds in response to changes in environmental conditions (Nelson *et al.*, 2002). Thus, virtually all compounds represent potential sources of carbon, nitrogen and/or energy upon transformation into central metabolic intermediates (Hou *et al.*, 2003). The ability to use novel chemicals, such as those recently produced by human activity, is thought to derive from unusual activities of pre-existing enzymes, from the altered reactivity of naturally arising enzyme isoforms or from horizontal gene transfer (Mandelbaum *et al.*, 1993; de Souza *et al.*, 1998; Wackett & Ellis, 1999; Ochman *et al.*, 2000; Seffernick & Wackett, 2001; Wackett & Hershberger, 2001; Johnson *et al.*, 2002). The structures, ancestry and regulation of enzymes that participate in newly emerged catabolic pathways have only infrequently been documented. However, these results are of interest because they impact diverse areas, including microbial drug resistance, bioremediation of priority pollutants and the evolution of enzyme structure and function (Davies, 1994; Mazel & Davies, 1999; Rieger *et al.*, 2002).

Nitrochemicals are an important class of chemicals that are used as drugs, biocides, fuels, explosives and solvents. Since nitro-group reduction can yield reactive nitrogen intermediates capable of modifying DNA, these compounds are considered to be mutagenic and toxic (Goldstein *et al.*, 1977; Sisson *et al.*, 2000, 2002; Sakano *et al.*, 2001; Homma-Takeda *et al.*, 2002). Consequently, the US Environmental Protection Agency regulates many sites contaminated with these molecules.

The nitro-containing explosives nitroglycerin and 2,4,6-trinitrotoluene (TNT) were first synthesized in 1846 and 1863, respectively, and have since become widely distributed in the environment. Their relatively recent introduction and unique chemical properties relative to naturally occurring compounds make them attractive examples for the study of the processes leading to xenobiotic transformation. Although no pathways for the complete aerobic catabolism of nitroglycerin or TNT are currently known, recent studies have established that these compounds are indeed transformed by a variety of enzymes to diverse products (Spain, 1995; Spain *et al.*, 2000; Rosser *et al.*, 2001). A documentation of the mechanisms by which these catabolic activities have emerged and continue to evolve would be of great interest. Toward this goal, the present work originated with the isolation of *Pseudomonas putida* II-B from nitro-contaminated soil at the Badger Army Ammunition Plant in Wisconsin, USA. This

bacterium was enriched by the ability to obtain all nitrogen required for growth from nitroglycerin through the reductive elimination of nitrite. This reaction is catalyzed by a monomeric 39 kDa flavin mononucleotide-containing enzyme called xenobiotic reductase A (XenA). It catalyzes the successive NADPH-dependent nitrite elimination of nitroglycerin, with an apparent preference for the removal of a terminal nitro group. XenA will also reduce the nitro groups of TNT and metronidazole and the double bond of 2-cyclohexenone to yield cyclohexanone (Blehert *et al.*, 1999; Pak *et al.*, 2000).

Here, we report the initial crystallization and analysis of X-ray diffraction data from the native XenA, selenomethionine-enriched (SeMet) XenA and ligand complexes formed by co-crystallization with nitroglycerin, TNT and metronidazole. The data are of sufficient quality to permit structural characterization.

2. Material and methods

2.1. Protein expression and purification

P. putida II-B was isolated as reported previously (Blehert *et al.*, 1997). XenA was cloned and expressed in *Escherichia coli* and purified as reported previously (Blehert *et al.*, 1997, 1999). The enzymes isolated from *P. putida* II-B and *E. coli* were indistinguishable. SeMet XenA was produced in *E. coli* B834 (DE3) using fed-batch fermentation (Studts & Fox, 1999) and purified as previously reported except that 5 m*M* DTT was added to all buffers (Blehert *et al.*, 1997, 1999). Mass-spectral analysis of the purified SeMet XenA showed that the N-terminal methionine was completely removed and that the average SeMet enrichment was approximately 95%.

2.2. Crystallization and X-ray data collection

The initial crystallization conditions for XenA were determined from a sparse-matrix approach and optimized using additive screens from Hampton Research (Laguna Nigel, CA, USA). Hanging drops were equilibrated by vapor diffusion in Linbro 24-well plates at room temperature in Styrofoam insulated boxes. Typically, 2 µl protein solution (5–10 mg ml^{-1} in 20 m*M* HEPES buffer pH 7.0) was mixed with either 2 µl reservoir solution or 2 µl reservoir solution plus 1 µl ligand solution on a silanized cover slip. XenA crystals (Fig. 1) were obtained from 0.1 *M* HEPES pH 7.4, 20 m*M* spermine tetrahydrochloride, 5% polyethylene glycol (PEG) 400 or PEG 8000 and 1.4–1.6 *M* ammonium sulfate. The ligand complexes of XenA were obtained by mixing SeMet XenA with nitroglycerin (1.1 m*M* final concentration from a 4.4 *M* stock solution dissolved in ethanol; VWR Inc.), TNT (2.2 m*M* final concentration from a 4.4 m*M* stock solution dissolved in acetonitrile; VWR Inc.) or metronidazole (16.4 m*M* final concentration from a 65.5 m*M* stock solution in water; ICN Biomedical Inc.) prior to setting up the hanging-drop experiment as above. Large single crystals required ∼3 d of undisturbed equilibration time. The crystals were harvested from the drop with nylon loops and transferred into a cryoprotectant, which was Paratone-N most often (Hampton Research). The crystals were centered in the loop and the excess mother liquor was removed by briskly pulling the viscous cryoprotectant away from the crystal along the long axis of the crystal habit. The crystals were flash-frozen by either plunging the

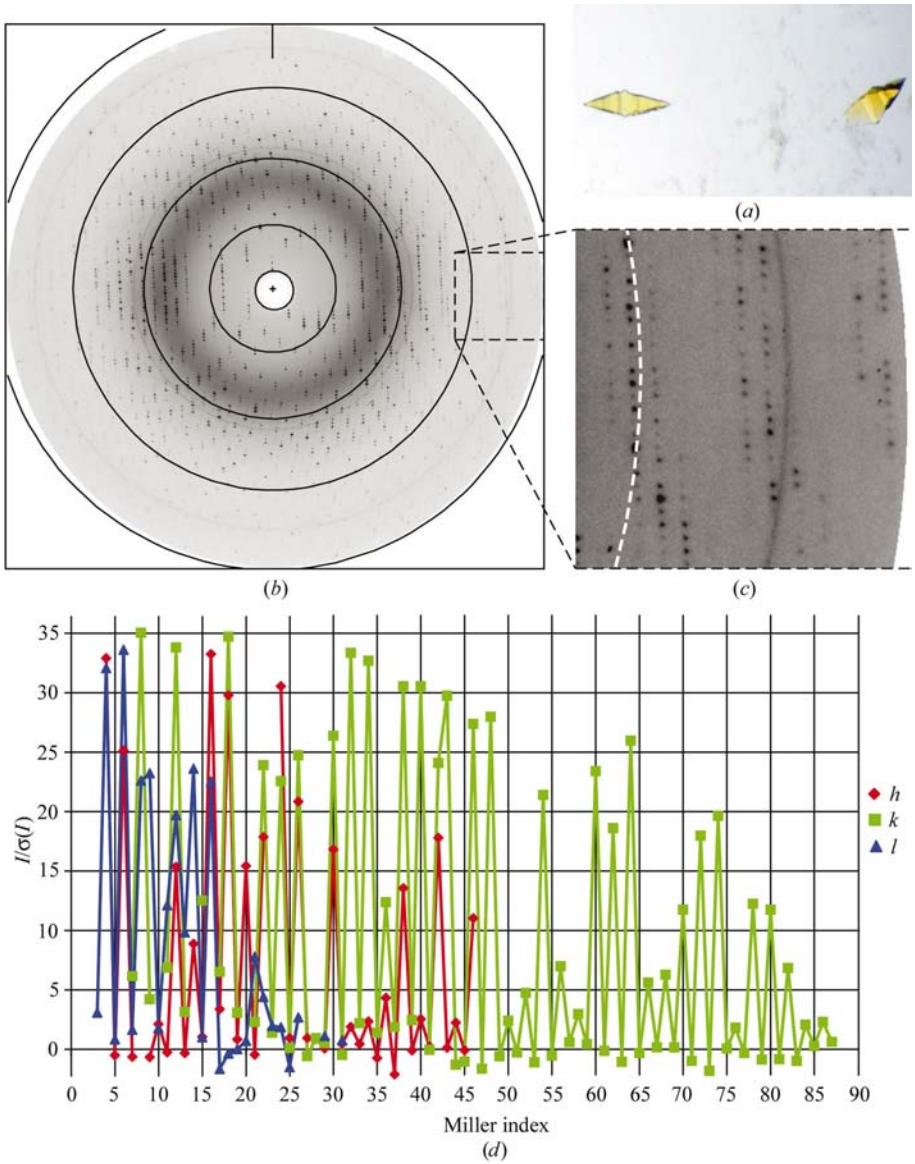

Figure 1
(*a*) Crystals (∼0.3 × 0.1 mm) of SeMet XenA grown in the presence of 1.1 m*M* nitroglycerin photographed without polarization. (*b*) The X-ray diffraction pattern obtained at 100 K from SER-CAT beamline 22-ID, 1 s exposure, 1° rotation about the vertical axis (vertical line), 150 mm crystal-to-detector distance, MAR CCD 165 detector. The arcs indicate 2.0, 2.7, 4.0, 8.0 and 28 Å resolution, respectively. (*c*) An expanded and contrast-adjusted view of the high-resolution diffraction perpendicular to the rotation axis. The dashed arc indicates 2.7 Å resolution. (*d*) Intensities of principal axis reflections for the XenA–metronidazole complex, which are typical of all data sets. Systematic absences along (*h*00) (red diamonds) and (0*k*0) (green squares) and pseudo-systematic absences along (00*l*) (blue triangles) are indicated by periodic $I/\sigma(I)$ values, which are the root-mean-square value of the intensity divided by the estimated standard deviation. The lines connecting the points are included solely to help illustrate the relationship between reflections along the each principal axis.

Table 1
Typical data-collection statistics for XenA.

Values for the highest resolution shell of data are given in parentheses.

		SeMet XenA						
	XenA	Inflection	Peak	Low-energy remote	High-energy remote	SeMet XenA, peak	SeMet XenA, remote	XenA
Ligand	—	—	—	—	—	1 m*M* nitroglycerin	1 m*M* TNT	16 m*M* metronidazole
X-ray source	SSRL	SSRL	SSRL	SSRL	SSRL	SER-CAT	SER-CAT	SER-CAT
Beamline	9-1	1-5	1-5	1-5	1-5	22-ID	22-ID	22-ID
Wavelength (Å)	0.98	0.979764	0.979609	1.06883	0.925256	0.979324	1.0332	1.0
Detector	MAR 345	Quantum 4R	Quantum 4R	Quantum 4R	Quantum 4R	MAR CCD 165	MAR CCD 165	MAR CCD 165
Temperature (K)	283	100	100	100	100	100	100	100
Resolution range (Å)	35.6–1.65	33.0–2.5	35.1–2.5	37.0–2.5	31.1–3.0	28.2–2.0	32.8–2.3	27.1–1.8
Mosaic spread (°)	∼0.2	∼0.6	∼0.6	∼0.6	∼0.6	∼0.9	∼1	∼0.9
Unit-cell parameters (Å)								
a	84.7	83.9	83.9	83.9	83.90	84.1	83.8	84.3
b	157.9	157.5	157.5	157.5	157.50	157.8	158.1	158.2
c	58.7	57.0	57.0	57.0	57.0	57.2	57.0	57.3
Total reflections	312545	171463	208342	194373	89489	318610	221776	347467
Unique reflections	94132	24191	24297	23455	13929	43335	32984	70825
Multiplicity	3.3 (3.3)	7.1 (7.0)	8.6 (8.5)	8.3 (6.7)	6.4 (6.4)	7.2 (4.9)	6.6 (5.6)	4.9 (5.4)
Completeness (%)	98.9 (98.9)	91.1 (91.1)	91.5 (91.5)	88.4 (88.4)	89.8 (89.8)	87.2 (70.0)	97.8 (95.9)	99.6 (99.2)
Anomalous completeness (%)	—	89.9 (90.0)	90.5 (91.2)	86.8 (64.0)	81.4 (84.5)	86.2 (56.9)	—	—
R_{sym}†	0.051 (0.39)	0.128 (0.497)	0.121 (0.442)	0.105 (0.369)	0.173 (0.478)	0.027 (0.138)	0.097 (0.325)	0.052 (0.316)
$I/\sigma(I)$‡	17.5 (4.5)	5.4 (1.5)	5.7 (1.7)	6.5 (2.0)	4.1 (1.6)	21.8 (4.1)	6.6 (2.3)	11.1 (2.5)

† $R_{sym}(I)$ gives the average agreement between the independently measured intensities such as $\sum_h \sum_i |I_i - I|/\sum_h \sum_i I_i$, where I is the mean intensity of the i observations of reflection h. ‡ $I/\sigma(I)$ is the root-mean-square value of the intensity measurements divided by their estimated standard deviation.

loop into liquid N_2 or by using the cold stream at the X-ray source. Several data sets were also collected at ∼283 K with a crystal mounted and sealed in a 0.3 mm glass capillary.

The X-ray diffraction data sets (Table 1) were collected at either the Stanford Synchrotron Radiation Laboratory or the Advanced Photon Source beamline 22-ID operated by the South East Regional Collaborative Access Team. The 283 K native data set was collected in one continuous 80° wedge of φ rotation with a MAR 345 image-plate detector and a 225 mm crystal-to-film distance. All other data sets were collected using CCD-based area detectors. Fluorescence scans of the SeMet XenA crystals were analyzed to select the peak, inflection point and high- and low-energy remote wavelengths. The MAD data set for Se-Met XenA was collected using the inverse-beam method; two wedges of φ rotation that covered all the unique area of reciprocal space and two complementary wedges of $\varphi + 180°$ were collected at each wavelength. The diffraction images were typically integrated with *MOSFLM* (Powell, 1999) and merged and scaled with *SCALA* from the *CCP*4 suite of programs (Collaborative Computational Project, Number 4, 1994). Occasionally, a data set was integrated with *HKL*2000 and scaled with *SCALEPACK* (Otwinowski & Minor, 1997). The data sets were further analyzed and merged with *FHSCAL* or *SCALEIT*. The SeMet XenA MAD data were analyzed with *SOLVE* (Terwilliger & Berendzen, 1999) to locate the Se sites using the theoretical X-ray scattering factors calculated for each wavelength (*CROSSEC*). The resulting sites were refined with respect to all four wavelengths of the MAD data set with *SHARP* (de La Fortelle & Bricogne, 1997). The solvent-flattened experimental maps revealed clearly interpretable density for two monomers in the asymmetric unit.

3. Results and discussion

Crystals of XenA exhibited an elongated bipyramidal habit (Fig. 1) that was easily oriented with the long axis parallel to the long axis of the cryoloop and consequently also with the goniometer φ-rotation axis. As indicated by the diffraction pattern for XenA aligned in this manner, the longest reciprocal cell axis was also aligned with the longest feature of the crystal habit. The X-ray diffraction data sets from XenA were all consistent with a primitive orthorhombic unit cell with approximate parameters 57, 84 and 158 Å (Table 1). Cryopreservation and co-crystallization of three potential ligand complexes did not significantly perturb the unit-cell parameters (Table 1). Upon assumption of a reasonable molecular weight per unit volume (V_M = 2.47 Å^3 Da^{-1} and 50% solvent content; Matthews, 1968), two XenA molecules were assigned per asymmetric unit. Analysis of self-rotation functions with *GLRF* v.1.1 (Tong & Rossmann, 1997) did not reveal any significant peaks in the κ = 90 or 120° sections and revealed three peaks (∼21σ) centered at (0, 0, 180°), (0, 90, 180°) and (90, 90, 180°) in the κ = 180° section. Therefore, the two molecules were likely to be related by at least twofold symmetry, which was also nearly parallel to a crystal unit-cell axis.

Primitive orthorhombic space groups are differentiated by the presence of crystallographic twofold screw axes. If present, 2_1 symmetry requires that odd reflections are systematically absent along the principal axis. Consequently, the observed $I/\sigma(I)$ of the principal axis reflections (when scaled in space group *P*222) strongly suggested that XenA crystallized in space group $P2_12_12_1$ (Fig. 1*d*). Indeed, the average $I/\sigma(I)$ for reflections along the three principal axes for the XenA–metronidazole complex are (even, 0, 0) = 14.55, (odd, 0, 0) = 0.14, (0, even, 0) = 17.35, (0, odd, 0) = 1.79, (0, 0, even) = 13.77 and (0, 0, odd) = 4.30. However, a few reflections along each principal axis in each data set violated the systematic absence condition; for example, in the XenA–metronidazole complex the reflection (17, 0, 0) has $I/\sigma(I)$ = 3.4, (0, 15, 0) = 15.4, (0, 43, 0) = 29.7, (0, 0, 9) = 23.2, (0, 0, 11) = 12.1 and (0, 0, 13) = 9.8. Therefore, an unambiguous determination of the space group was not possible using only the observed reflections along the three principal axes.

Furthermore, analysis of the SeMet XenA MAD data with *SOLVE* v.1.16 did not yield reasonable solutions in space group $P2_12_12_1$. In the best case, only three Se sites (of an expected ten sites) were located with a figure of merit of 0.32, a *Z* score of 38.2 and an

Table 2
Relationship between the five Se sites in each XenA molecule in the asymmetric unit.

Se Site	Observed Se coordinates (molecule *A*)†	Observed Se coordinates (molecule *B*)†	Molecule *A* sites after 2_1 transformation‡ ($A2_1$)	$B-A2_1$§ (Å)	$B-A2_1$¶ (% of unit cell)
1	$x = 35.38$	$x = 8.43$	$x = 6.59$	$\Delta x = 1.84$	$\lvert\Delta x\rvert = 2.19a$
	$y = 58.27$	$y = 19.86$	$y = 20.47$	$\Delta y = -0.61$	$\lvert\Delta y\rvert = 0.39b$
	$z = 12.07$	$z = 40.12$	$z = 40.56$	$\Delta z = -0.44$	$\lvert\Delta z\rvert = 0.78c$
2	$x = 31.73$	$x = 11.82$	$x = 10.23$	$\Delta x = 1.59$	$\lvert\Delta x\rvert = 1.90a$
	$y = 60.67$	$y = 17.26$	$y = 18.07$	$\Delta y = -0.81$	$\lvert\Delta y\rvert = 0.51b$
	$z = 7.74$	$z = 35.54$	$z = 36.23$	$\Delta z = -0.69$	$\lvert\Delta z\rvert = 1.20c$
3	$x = 18.23$	$x = 24.44$	$x = 23.73$	$\Delta x = 0.71$	$\lvert\Delta x\rvert = 0.85a$
	$y = 69.25$	$y = 7.41$	$y = 9.49$	$\Delta y = -2.08$	$\lvert\Delta y\rvert = 1.32b$
	$z = 5.71$	$z = 33.66$	$z = 34.20$	$\Delta z = -0.54$	$\lvert\Delta z\rvert = 0.95c$
4	$x = 40.12$	$x = 4.18$	$x = 1.84$	$\Delta x = 2.34$	$\lvert\Delta x\rvert = 2.79a$
	$y = 51.09$	$y = 27.59$	$y = 27.65$	$\Delta y = -0.06$	$\lvert\Delta y\rvert = 0.04b$
	$z = 0.78$	$z = 28.40$	$z = 29.27$	$\Delta z = -0.87$	$\lvert\Delta z\rvert = 1.53c$
5	$x = 12.55$	$x = 32.27$	$x = 29.41$	$\Delta x = 2.86$	$\lvert\Delta x\rvert = 3.40a$
	$y = 46.261$	$y = 29.83$	$y = 32.48$	$\Delta y = -2.65$	$\lvert\Delta y\rvert = 1.69b$
	$z = 52.01$	$z = 23.01$	$z = 23.52$	$\Delta z = -0.51$	$\lvert\Delta z\rvert = 0.88c$

† The position of the Se atoms in the asymmetric unit after refinement by *SHARP*. ‡ Location of the Se atoms after a 2_1 symmetry transformation of the molecule *A* sites. § Distance between the Se sites of molecule *B* and the 2_1 symmetry-transformed Se sites of molecule *A*. ¶ The same distance between sites, but normalized to a percentage of the given unit-cell parameter.

average peak height/σ of 11.6. Consequently, the data were systematically re-indexed into the other orthorhombic space groups with permutations of the unit-cell parameters. Reproducible results with *SOLVE* were only obtained in space group $P2_12_12$, with $a = 84$, $b = 158$, $c = 57$ Å. For example, using a subset of the MAD data comprised of the inflection, peak and low-energy remote wavelengths and reflections between 3.0 and 35 Å resolution, nine Se sites were located with a maximum and minimum peak height/σ of 20.3 and 11.1, respectively, and an average of 14.9. The figure of merit for this solution was 0.39 and the *Z* score was 27.8. The nine original Se sites refined to convergence with the four-wavelength data set in *SHARP*. A greater than $+5\sigma$ difference peak clearly indicated the tenth Se site, which superimposed with the tenth Se site determined by analysis with *SOLVE*. The phasing statistics included a phasing power of 2.78 for centric reflections between 2.5 and 30 Å resolution using the peak wavelength (0.979609 Å). The overall figure of merit was 0.471 for 2437 centric reflections and 0.493 for 22 091 acentric reflections, which improved to 0.808 (22 966 reflections) after solvent flattening. The resulting electron-density maps were clearly interpretable and of sufficient quality for complete model building.

The ten refined Se sites in the asymmetric unit were also used to determine the non-crystallographic symmetry between the two XenA molecules in the asymmetric unit. Application of a 2_1 symmetry operator to chain *A* yielded sites that could be compared with the observed locations of Se atoms in chain *B*. As illustrated in Table 2, only small differences were identified between crystallographic 2_1 symmetry and the observed local symmetry. Therefore, the local symmetry can be described as a 2_1 screw axis which is displaced approximately one-quarter off and nearly parallel to the *c* axis (Table 2). Consequently, the resulting local symmetry yields intensities along (00*l*) that can be described as pseudo-systematic absences.

Primary sequence analyses, catalytic studies and the emerging structural results indicate that XenA is a member of the FMN-dependent oxidoreductase subfamily of the $(\beta/\alpha)_8$ TIM-barrel superfamily (Blehert *et al.*, 1997, 1999; Pak *et al.*, 2000; Nagano *et al.*, 2002). XenA shares 27% identity and 44% similarity with old yellow enzyme (OYE), the prototypical member of the subfamily (Fox & Karplus, 1994, 1999; Massey, 2000), while other structurally characterized members of this subfamily include pentaerythritol tetranitrate reductase (Khan *et al.*, 2002), 2,4-dienoyl-CoA reductase (Hubbard *et al.*, 2003), morphinone reductase (Barna *et al.*, 2002) and the 12-oxophytodienoate reductase isoforms 1 (Breithaupt *et al.*, 2001) and 3 (PDB code 1q45). Several unsuccessful molecular-replacement attempts were made with search models comprised of OYE and other homologs. All of these enzymes are capable of the reduction of unsaturated carbonyl compounds. Thus, it appears that XenA may have evolved from an ancestral enzyme that catalyzed a similar reaction, but structural differences are also likely to be present. More detailed comparisons between the structure, function and evolution of these enzymes will be presented elsewhere. The phases from the refined XenA structure have been used to calculate electron-density maps that are consistent with ligands such as metronidazole in the active site.

Diffraction data were collected at the Stanford Synchrotron Radiation Laboratory (Stanford University, supported by the Department of Energy, Office of Biological and Environmental Research, the National Institutes of Health, National Center for Research Resources, Biomedical Technology Program and the National Institute of General Medical Sciences) and beamline 22-ID of the SER-CAT facility at the Advanced Photon Source, Argonne National Laboratory (supported by the US Department of Energy, Basic Energy Sciences, Office of Science under Contract No. W-31-109-Eng-38). Support was provided to AMO by the Georgia Tech Research Corporation, the Office of the Vice Provost for Research and the Howard Hughes Medical Institutes (from Dr B. W. Matthews, Institute of Molecular Biology, Howard Hughes Medical Institute and Department of Physics, 1229 University of Oregon, Eugene, Oregon). Support was provided to BGF from NSF MCB-9733734.

References

Barna, T., Messiha, H. L., Petosa, C., Bruce, N. C., Scrutton, N. S. & Moody, P. C. (2002). *J. Biol. Chem.* **277**, 30976–30983.
Blehert, D. S., Fox, B. G. & Chambliss, G. H. (1999). *J. Bacteriol.* **181**, 6254–6263.
Blehert, D. S., Knoke, K. L., Fox, B. G. & Chambliss, G. H. (1997). *J. Bacteriol.* **179**, 6912–6920.
Breithaupt, C., Strassner, J., Breitinger, U., Huber, R., Macheroux, P., Schaller, A. & Clausen, T. (2001). *Structure*, **9**, 419–429.
Collaborative Computational Project, Number 4 (1994). *Acta Cryst.* D**50**, 760–763.
Davies, J. (1994). *Science*, **264**, 375–382.
Falkowski, P., Scholes, R. J., Boyle, E., Canadell, J., Canfield, D., Elser, J., Gruber, N., Hibbard, K., Hogberg, P., Linder, S., Mackenzie, F. T., Moore, B. III, Pedersen, T., Rosenthal, Y., Seitzinger, S., Smetacek, V. & Steffen, W. (2000). *Science*, **290**, 291–296.
Fox, K. M. & Karplus, P. A. (1994). *Structure*, **2**, 1089–1105.
Fox, K. M. & Karplus, P. A. (1999). *J. Biol. Chem.* **274**, 9357–9362.
Goldstein, B. P., Nielsen, E., Berti, M., Bolzoni, G. & Silvestri, L. G. (1977). *J. Gen. Microbiol.* **100**, 271–281.
Homma-Takeda, S., Hiraku, Y., Ohkuma, Y., Oikawa, S., Murata, M., Ogawa, K., Iwamuro, T., Li, S., Sun, G. F., Kumagai, Y., Shimojo, N. & Kawanishi, S. (2002). *Free Radic. Res.* **36**, 555–566.
Hou, B. K., Wackett, L. P. & Ellis, L. B. (2003). *J. Chem. Inf. Comput. Sci.* **43**, 1051–1057.
Hubbard, P. A., Liang, X., Schulz, H. & Kim, J. J. (2003). *J. Biol. Chem.* **278**, 37553–37560.

Johnson, G. R., Jain, R. K. & Spain, J. C. (2002). *J. Bacteriol.* **184**, 4219–4232.
Khan, H., Harris, R. J., Barna, T., Craig, D. H., Bruce, N. C., Munro, A. W., Moody, P. C. & Scrutton, N. S. (2002). *J. Biol. Chem.* **277**, 21906–21912.
La Fortelle, E. de & Bricogne, G. (1997). *Methods Enzymol.* **276**, 472–494.
Mandelbaum, R. T., Wackett, L. P. & Allan, D. L. (1993). *Appl. Environ. Microbiol.* **59**, 1695–1701.
Massey, V. (2000). *Biochem. Soc. Trans.* **28**, 283–296.
Matthews, B. W. (1968). *J. Mol. Biol.* **33**, 491–497.
Mazel, D. & Davies, J. (1999). *Cell. Mol. Life Sci.* **56**, 742–754.
Mojzsis, S. J., Arrhenius, G., McKeegan, K. D., Harrison, T. M., Nutman, A. P. & Friend, C. R. (1996). *Nature (London)*, **384**, 55–59.
Nagano, N., Orengo, C. A. & Thornton, J. M. (2002). *J. Mol. Biol.* **321**, 741–765.
Nelson, K. E. *et al.* (2002). *Environ. Microbiol.* **4**, 799–808.
Nisbet, E. G. & Sleep, N. H. (2001). *Nature (London)*, **409**, 1083–1091.
Ochman, H., Lawrence, J. G. & Groisman, E. A. (2000). *Nature (London)*, **405**, 299–304.
Otwinowski, Z. & Minor, W. (1997). *Methods Enzymol.* **276**, 307–326.
Pak, J. W., Knoke, K. L., Noguera, D. R., Fox, B. G. & Chambliss, G. H. (2000). *Appl. Environ. Microbiol.* **66**, 4742–4750.
Powell, H. R. (1999). *Acta Cryst.* D**55**, 1690–1695.
Rieger, P. G., Meier, H. M., Gerle, M., Vogt, U., Groth, T. & Knackmuss, H. J. (2002). *J. Biotechnol.* **94**, 101–123.
Rosser, S. J., Basran, A., Travis, E. R., French, C. E. & Bruce, N. C. (2001). *Adv. Appl. Microbiol.* **49**, 1–35.
Sakano, K., Oikawa, S., Murata, M., Hiraku, Y., Kojima, N. & Kawanishi, S. (2001). *Mutat. Res.* **479**, 101–111.
Seffernick, J. L. & Wackett, L. P. (2001). *Biochemistry*, **40**, 12747–12753.
Sisson, G., Goodwin, A., Raudonikiene, A., Hughes, N. J., Mukhopadhyay, A. K., Berg, D. E. & Hoffman, P. S. (2002). *Antimicrob. Agents Chemother.* **46**, 2116–2123.
Sisson, G., Jeong, J. Y., Goodwin, A., Bryden, L., Rossler, N., Lim-Morrison, S., Raudonikiene, A., Berg, D. E. & Hoffman, P. S. (2000). *J. Bacteriol.* **182**, 5091–5096.
Souza, M. L. de, Seffernick, J., Martinez, B., Sadowsky, M. J. & Wackett, L. P. (1998). *J. Bacteriol.* **180**, 1951–1954.
Spain, J. C. (1995). *Annu. Rev. Microbiol.* **49**, 523–555.
Spain, J. C., Hughes, J. B. & Knackmuss, H. J. (2000). *Biodegradation of Nitroaromatic Compounds and Explosives.* Boca Raton, FL, USA: CRC Press.
Studts, J. M. & Fox, B. G. (1999). *Protein Expr. Purif.* **16**, 109–119.
Terwilliger, T. C. & Berendzen, J. (1999). *Acta Cryst.* D**55**, 849–861.
Tong, L. & Rossmann, M. G. (1997). *Methods Enzymol.* **276**, 594–611.
Wackett, L. P. & Ellis, L. B. (1999). *Environ. Microbiol.* **1**, 119–124.
Wackett, L. P. & Hershberger, C. D. (2001). *Biocatalysis and Biodegradation: Microbial Transformation of Organic Compounds.* Washington, DC, USA: ASM Press.
Watanabe, Y., Martini, J. E. & Ohmoto, H. (2000). *Nature (London)*, **408**, 574–578.